Journal of Colloid and Interface Science 448 (2015) 582–592

Contents lists available at ScienceDirect

Journal of Colloid and Interface Science

www.elsevier.com/locate/jcis

Synthesis and thermal stability of zirconia and yttria-stabilized zirconia microspheres

Elisabeth W. Leib [a], Ulla Vainio [b], Robert M. Pasquarelli [c], Jonas Kus [a], Christian Czaschke [a], Nils Walter [a], Rolf Janssen [c], Martin Müller [b], Andreas Schreyer [b], Horst Weller [a,d,e], Tobias Vossmeyer [a,*]

[a] Institute of Physical Chemistry, University of Hamburg, Grindelallee 117, D-20146 Hamburg, Germany
[b] Institute of Materials Research, Helmholtz-Zentrum Geesthacht, Max-Planck-Straße 1, 21502 Geesthacht, Germany
[c] Institute of Advanced Ceramics, Hamburg University of Technology (TUHH), Denickestraße 15, 21073 Hamburg, Germany
[d] The Hamburg Centre for Ultrafast Imaging, Luruper Chaussee 149, 22761 Hamburg, Germany
[e] Department of Chemistry, Faculty of Science, King Abdulaziz University, Jeddah, Saudi Arabia

GRAPHICAL ABSTRACT

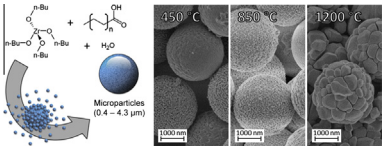

ARTICLE INFO

Article history:
Received 10 November 2014
Accepted 20 February 2015
Available online 27 February 2015

Keywords:
Ceramic
Microspheres
Thermal barrier coating
Phase transformation
Zirconia
YSZ

ABSTRACT

Hypothesis: Zirconia microparticles produced by sol–gel synthesis have great potential for photonic applications. To this end, identifying synthetic methods that yield reproducible control over size uniformity is important. Phase transformations during thermal cycling can disintegrate the particles. Therefore, understanding the parameters driving these transformations is essential for enabling high-temperature applications. Particle morphology is expected to influence particle processability and stability. Yttria-doping should improve the thermal stability of the particles, as it does in bulk zirconia.

Experiments: Zirconia and YSZ particles were synthesized by improved sol–gel approaches using fatty acid stabilizers. The particles were heated to 1500 °C, and structural and morphological changes were monitored by SEM, *ex situ* XRD and high-energy *in situ* XRD.

Findings: Zirconia particles (0.4–4.3 μm in diameter, 5–10% standard deviation) synthesized according to the modified sol–gel approaches yielded significantly improved monodispersities. As-synthesized amorphous particles transformed to the tetragonal phase at ~450 °C with a volume decrease of up to ~75% and then to monoclinic after heating from ~650 to 850 °C. Submicron particles disintegrated at ~850 °C and microparticles at ~1200 °C due to grain growth. *In situ* XRD revealed that the transition from the amorphous to tetragonal phase was accompanied by relief in microstrain and the transition from tetragonal to monoclinic was correlated with the tetragonal grain size. Early crystallization and smaller initial grain sizes, which depend on the precursors used for particle synthesis, coincided with higher stability. Yttria-doping reduced grain growth, stabilized the tetragonal phase, and significantly improved the thermal stability of the particles.

1. Introduction

Mesoscale-structured zirconia ceramics combine many favorable properties such as a low thermal conductivity, high chemical and thermal stability, and high refractive index [1–3], and are

* Corresponding author. Fax: +49 (0)40 42838 3452.
E-mail address: tobias.vossmeyer@chemie.uni-hamburg.de (T. Vossmeyer).

http://dx.doi.org/10.1016/j.jcis.2015.02.049
0021-9797/

attractive for applications such as fuel cells [4,5], catalysis [6–8], sensors [9,10], bioseparation [11], and chromatography [12–15]. Besides their possible use in catalysis and chromatography, materials composed of spherical zirconia particles in the micrometer range can enable photonic properties when the particles are arranged into ordered [16] or disordered [17,18] structures. Such photonic structures have attracted increasing interest for high-temperature applications, including advanced thermal barrier coatings (TBCs) [19], heat-resistant structural colorants [20] and substrates for metallo-dielectric absorbers/emitters used in thermophotovoltaics [21]. Recently, we demonstrated that films composed of disordered, monodisperse, micrometer-sized zirconia particles, whose synthesis and stability will be discussed herein, function as efficient broadband reflectors in the infrared spectrum (1–6 μm) [22].

In these applications, the synthesis and processing of the particles must meet several criteria. For chromatography, the particles must achieve reproducible performance, and identifying methods of synthesis that yield reproducible control of size uniformity and an understanding of how the particles deteriorate are important. For photonic applications, the particles must fulfill several additional criteria. Firstly, the particles must be spherical and highly monodisperse, ideally with standard deviations below 5%. Aside from desired optical effects, this is especially important for achieving the self-assembly of ordered structures. Thus, agglomeration and secondary nucleation must be avoided during preparation. Second, applications in the NIR/IR range require the synthesis of larger microspheres, as the wavelength of the reflected light is directly proportional to the particle diameter. For ordered photonic crystals, the particle size governs the periodicity of the structure and thus the wavelength that will be Bragg diffracted. For disordered photonic glasses, resonant behaviors of electromagnetic modes occur when the wavelength of light is comparable with the sphere diameter (Mie scattering) [17,18]. Thus, TBCs require microparticles with diameters in the order of 3 μm to achieve reflection in the IR. Lastly, the particles must be high-temperature stable in order to maintain the photonic effects when cycling between room temperature and their working temperature (>1000 °C). This is particularly challenging in the case of undoped zirconia, which, in its bulk form, exhibits a martensitic tetragonal-to-monoclinic phase transformation when cooling below 1170 °C with an accompanying volume expansion of 3–5% [23]. In bulk zirconia, doping with yttrium, magnesium or calcium ions stabilizes the high-temperature tetragonal or cubic phase at room temperature.

To date, spherical zirconia submicron and micrometer particles have been prepared from zirconium salts [24–27], from sols *via* polymer-induced colloid aggregation [15,28–30] and from alkoxides *via* sol–gel processes [12,13,31–37]. Early synthetic approaches on utilizing a sol–gel route were developed by Fegley et al. [31,32]. Based on their findings, Ogihara et al. reported on the synthesis of microparticles with a diameter of 1 μm [33] and investigated their growth mechanism [34]. During the reaction, hydrolysis and polymerization results in the formation of primary grains of 10–20 nm in size, which then aggregate to form larger microspheres. By introducing fatty acids as stabilizers, Lerot et al. and Yan et al. were able to fine tune the microparticle size from 0.1 to 2.5 μm and 0.8 to 3.6 μm, respectively [12,13,35]. Widoniak et al. have also demonstrated stabilization and tunability with salts and polymers [36,37]. The main focus of these studies was the fabrication of powders for enhanced densification and grain growth in ceramic materials [26,32,35], and the use of zirconia spheres in catalysis [27] or as a stationary phase in chromatography [29]. The particles were heated to temperatures between 350 and 1000 °C. However, current trends in high-temperature applications of photonic materials require a clear understanding of particle morphology, stability and crystal structure and the effect of prolonged heating at temperatures above 1000 °C. In the case of yttria-stabilized zirconia (YSZ) particles, they have previously been synthesized using either yttrium nitrate or isopropoxide, but their maximum diameters were only 500 nm and the particles displayed low degrees of monodispersity [38,39]. These particles have been heated up to 1000 °C but an assessment of their stability at higher temperatures is likewise missing.

In this work, we address three key points. First, we outline the synthesis of zirconia particles with improved monodispersity from two modified sol–gel approaches using carboxylic acid stabilizers, which yielded consistently low standard deviations in size of 5–10%. Second, as all synthetic methods yield microspheres composed of smaller grains, it is important to understand the effects of this morphology on processability and phase stability for high-temperature applications. While it is well known that strain affects the phase stability of zirconia crystallites [40], a systematic investigation of the effects in microparticles prepared *via* the sol–gel method is lacking. Herein, we present the first in depth study of the influence of crystallite size and strain on the thermal stability of zirconia microparticles with sizes ranging from 0.8 to 4.3 μm. The crystalline phases and particle morphology were investigated *ex situ* after heating the particles up to 1500 °C. Using high-energy X-ray diffraction (HE-XRD), we were able to monitor the phase transitions *in situ*, and structural parameters such as monoclinic phase weight fraction, crystallite sizes and microstrain were determined. Third, we introduce a facile approach for the synthesis of monodisperse, yttria-stabilized microparticles with diameters of up to 2 μm and demonstrate their significantly improved high-temperature stability.

2. Experimental section

2.1. Particle synthesis

Submicron zirconia particles with diameters from 0.4 to 0.8 μm (before calcination) were prepared based on the sol–gel approach reported by Widoniak et al. [36]. The procedure was modified by using carboxylic acids of various chain lengths, rather than salts, as stabilizers in low concentration (1.8 mmol/L, corresponding to a stabilizer-to-zirconia ratio of 1:38) and by gently stirring the suspension throughout the ageing time instead of continuing with vigorous stirring or stopping the agitation. Zirconia microparticles with diameters between 2.8 and 4.3 μm (before calcination) were synthesized using a modification of the Yan method [13]. The reaction was carried out at 50 °C and, after the induction time had passed, the reaction vessel was transferred to a tube roller and the suspension was aged between 90 and 120 min. Yttria-stabilized zirconia microparticles were synthesized analogously to the synthesis of the larger microparticles with the addition of 600 mg (2.26 mmol) yttrium isopropoxide. The yttrium precursor was mixed with 12.2 g (26.1 mmol) zirconium n-propoxide (70% in n-propanol) and 10 mL anhydrous n-propanol, homogenized, filtered and added to the solution of eicosanoic acid in butanol. A detailed description of all synthetic procedures is provided in the Supplementary Material.

2.2. Ex situ heating and characterization

The particle samples were subjected to heat treatments in a muffle oven (L9/SKM, Nabertherm) and in a tube furnace (STF 16/100, Carbolite). The particles were then characterized by X-ray diffraction (XRD, Philips X'Pert PRO MPD), scanning electron microscopy (SEM, EVO MA 10 and a Leo Type 1550 Gemini, both Zeiss), thermogravimetry (TGA 209 F1 Iris from NETZSCH-Gerätebau) and inductively coupled plasma optical emission spectroscopy (ICP-OES, Spectro Model ARCOS spectrometer). The

heating rate profiles and details of these measurements are provided in the Supplementary Material (Figs. S6 and S7).

2.3. In situ heating and HE-XRD

High-energy X-ray diffraction experiments were carried out *in situ* at the HEMS beamline (P07) in the experimental hutch EH1 at the PETRA III synchrotron storage ring. The samples were heated with a focusing infrared lamp (Osram Xenophot 64635 HLX, 150W) up to 1170 °C. Details of these measurements and of the data analysis performed with the Maud software [41], as well as the heating rate profiles are provided in the Supplementary Material (Fig. S9 and Table S2).

3. Results and discussion

3.1. Synthesis of submicron and microparticles

Submicron zirconia particles were synthesized using the general method introduced by Widoniak et al. [36,37]. Building upon previous work of Ogihara et al. [33,34] and Kumazawa et al. [42], Widoniak et al. found that the particle size and monodispersity can be controlled by addition of stabilizers (salts or polymers) [36,37]. Here, we combined their method with the methods of Lerot et al. [35] and Yan et al. [12,13], who used fatty acids as stabilizers, and modified the reaction conditions and purification procedure, as detailed in the Supplementary Material. Carboxylic acids as stabilizers have an advantage over alkali halide salts in that they can easily be removed by subsequent calcination without leaving behind ionic impurities. Cationic and anionic impurities in zirconia particles have been shown to influence their crystallization behavior and susceptibility towards phase transformation and to increase surface area and porosity [43,44]. Using this optimized protocol we were able to synthesize submicron particles with a twofold improvement monodispersity, i.e. with size standard deviations ranging from 5% to 7%, compared to 10% to 15% reported previously [36,37].

It is generally accepted that the particles are formed in a two-step mechanism [33,34,36]. First, the alkoxide precursors are hydrolyzed and polymerized to form small primary particles in the size range of 10–20 nm, which then aggregate to form the final particles. In order to free the sample from residual primary particles and the results of possible secondary nucleation, the particles were separated and washed by centrifugation and subsequent resuspension in ethanol by ultrasonication. It was found that centrifugation at 0 °C instead of room temperature leads to less agglomeration.

In our present study we explored the effect of varying the chain lengths of the carboxylic acid stabilizers (C14–C28) on resulting particle sizes and monodispersities. Fig. 1 shows the zirconia particle diameter and the induction time as a function of the stabilizer chain length. The induction time, i.e. the time required for primary particle growth to initiate, is visibly indicated by the change of the solution from transparent to white. For carboxylic acids with chain lengths ranging from C6 to C18 [35] and C10 to C20 [13], increasing the alkane chain length has been reported to decrease the induction time and increase particle size. Similarly, when increasing the chain length from C14 to C24 we observed a decrease in induction time, which indicates an increase in hydrolysis rate, as shown in Fig. 1. In contrast to previous work [13,35] however, the particle diameter remained nearly constant at ~700 nm when increasing the stabilizer chain length from C14 to C20 and decreased to ~400 nm when further increasing the chain length from C24 to C28 (Fig. 1). The choice of stabilizer was also found to influence the monodispersity of the particles. Stearic (C18) and eicosanoic (C20) acid gave better monodispersity with standard deviations ranging between 5% and 7%. The standard deviations for samples

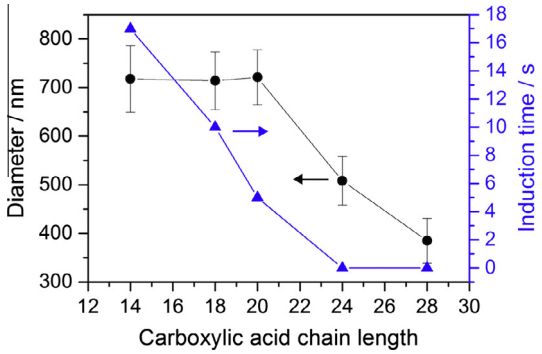

Fig. 1. Particle diameter and induction time as a function of the alkane chain length of the carboxylic acid stabilizer from C14 to C28. Error bars represent the standard deviations of the samples. An increase of the stabilizer chain length is accompanied by faster hydrolysis as indicated by the shorter induction times and by decreasing particle diameters.

prepared with tetradecanoic (C14), tetracosanoic (C24) and octacosanoic (C28) acid were 10%, 10% and 12%, respectively. As it gave better monodispersity, particles for further thermal stability experiments were synthesized using stearic and eicosanoic acid as stabilizers. Varying the alkane chain lengths is a convenient way of adapting the particle size without the use of alkali halide salts as stabilizers.

For the synthesis of larger zirconium dioxide microparticles, a modified version of the method by Yan et al. [12,13], which is based on the works of van Cantfort et al. [45] and Lerot et al. [35], was used. As described in detail in the Supplementary Material, adjusting the reaction temperature and agitation, and using short ageing times to avoid agglomeration and secondary nucleation, enabled the preparation of particles with diameters ranging from 2.8 and 4.3 μm with standard deviations of 6–10%. SEM images indicate that our modified protocol yielded smoother particle surfaces when eicosanoic acid was used instead of stearic acid (see Supplementary Material – Fig. S3). High monodispersity and smoother particle surfaces, as seen in Fig. 2, are useful for the packing and formation of ordered, defect-free structures during the assembly processes of photonic materials.

Using the optimized synthetic methods outlined above six particle samples, including two sets of the small particles (submicron particle synthesis) and of medium and large particles (microparticle synthesis), were prepared for *ex situ* and *in situ* heating experiments. The as-synthesized particles (i.e. before calcination) used for the *ex situ* experiments had diameters of 0.86 μm ± 5.3%, 2.8 μm ± 7.0% and 4.2 μm ± 6.0% and will subsequently be referred to as samples A0.86, B2.8 and C4.2, respectively. The diameters were measured using SEM micrographs by counting 200 particles per batch with the software ImageJ. The size distributions of A0.86, B2.8 and C4.2 are shown in Fig. 2. Analogously, the particles (before calcination) for the *in situ* experiments had diameters of 0.81 μm ± 6.7%, 2.8 μm ± 6.6% and 4.3 μm ± 9.7% and are referred to as samples D0.81, E2.8 and F4.3, respectively (Supplementary Material – Figs. S1 and S2). The similarity of the diameters and the consistently low standard deviations (5–10%) demonstrate the good reproducibility of the syntheses. The SEM images of the samples in Fig. 2 show that the particles are spherical, with smooth, regular surfaces, and display little agglomeration and secondary nucleation.

3.2. Ex situ experiments

3.2.1. Particle shrinkage

For many ceramic coating applications, such as thermal barrier coatings, it is necessary to avoid the formation of cracks, as this

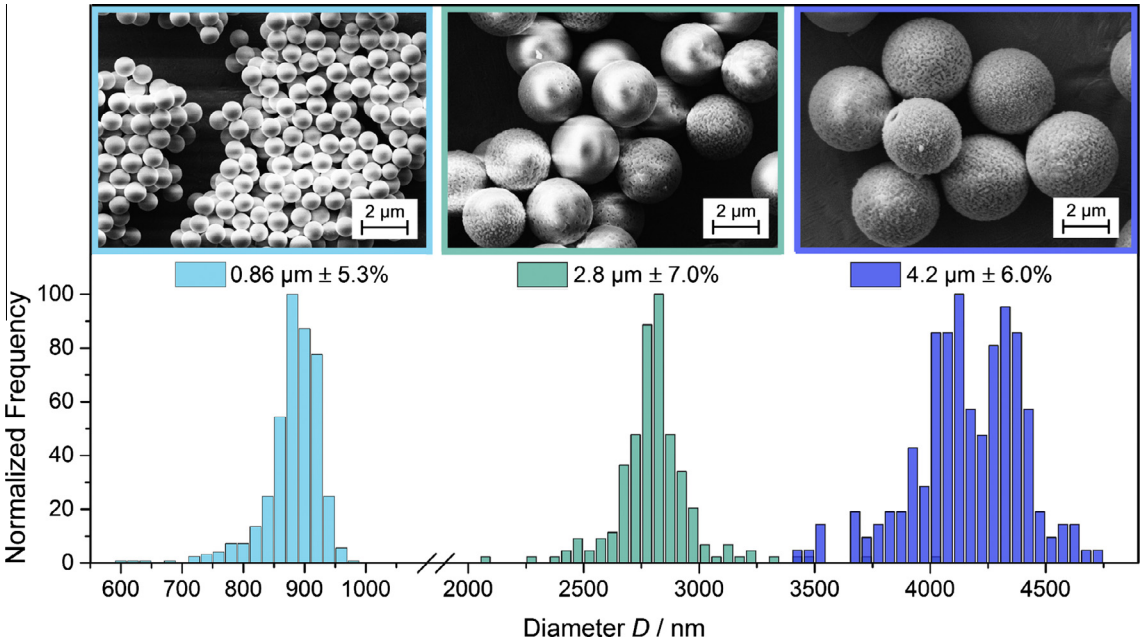

Fig. 2. Size distributions of as-synthesized small, medium and large particles for *ex situ* experiments, subsequently referred to as samples A0.86, B2.8 and C4.2. Corresponding SEM images of the particles are provided as insets.

leads to degradation of the material's optical properties. Hence, it is of vital importance to know the degree of shrinkage upon heating the particles. In order to investigate particle shrinkage after calcination, samples A0.86, B2.8 and C4.2 (dried at 80 °C for 4 h) were heated at temperatures of 250, 450, 650 and 850 °C for 1 h and cooled to room temperature for characterization. For each particle size and temperature, 100 particles were measured by SEM in order to determine the average diameter. Measurements of the initial particle diameters shown in Fig. 3 were carried out on unheated as-synthesized samples. Particle diameters and calculated volumes as a function of the calcination temperature in air are shown in Fig. 3(a) and (b). Thermogravimetric (TG) analysis of the particles (dried at 80 °C for 4 h) was also conducted (Supplementary Material – Fig. S5) and their mass loss under heating in air is shown in Fig. 3(c).

The as-synthesized samples most likely contained some residual water and zirconium hydroxide, besides the oxide. Therefore, the first mass loss event observed when heating the samples to 250 °C is most likely mainly due to loss of water. In all samples, the main decrease in diameter was seen between 250 and 450 °C with a decrease of 13%, 37% and 35% for A0.86, B2.8 and C4.2, respectively. This agrees well with the main mass loss event in the TG curves, corresponding to the decomposition temperatures of the precursors and stabilizers stearic acid (370 °C) and eicosanoic acid (328 °C). This decomposition was accompanied by crystallization of the particles from an amorphous phase at 250 °C to tetragonal zirconia at 450 °C as determined by XRD (Fig. 4). Heating above 450 °C did not result in a significant further change in diameter or mass loss. In previous studies it was reported that zirconia particles synthesized using fatty acids as stabilizers are

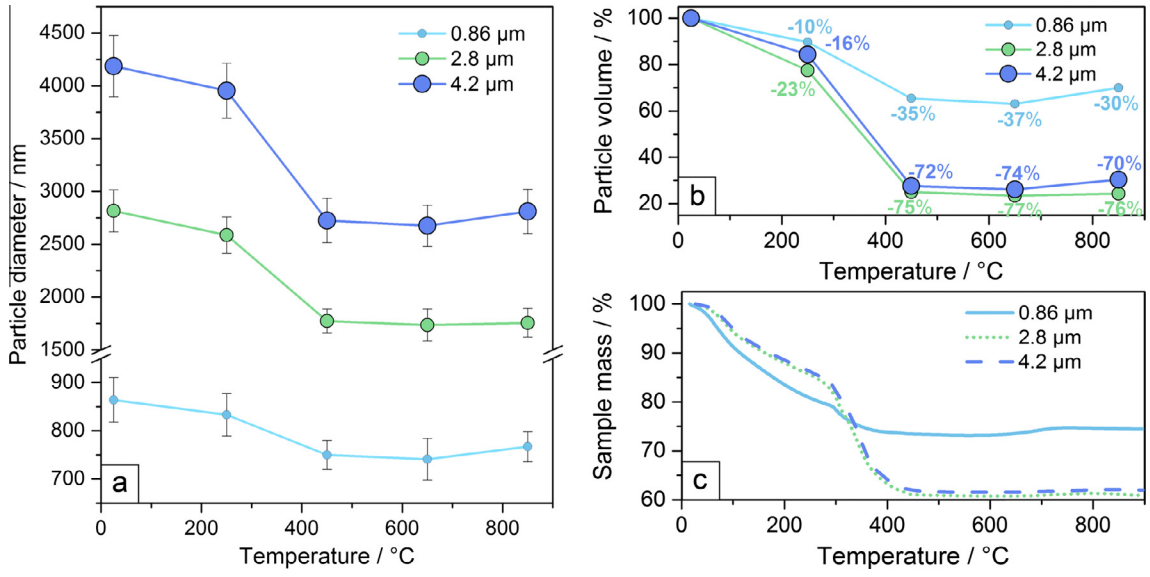

Fig. 3. Particle diameters of samples A0.86, B2.8 and C4.2 with standard deviations (a) and percent volume (b) as a function of the calcination temperature in air. Thermogravimetric analysis of particles in air (c). All three samples showed substantial mass loss between 250 and 450 °C and remained stable in size when heated above 450 °C.

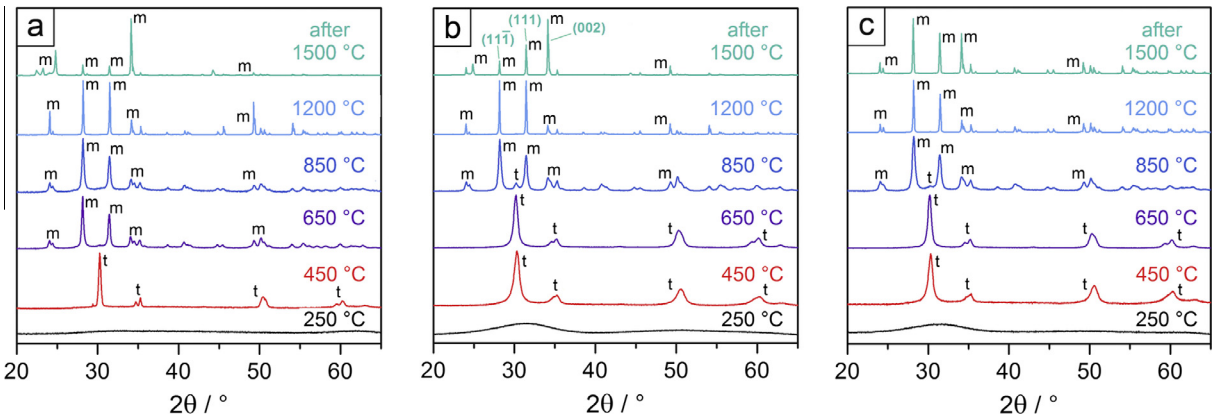

Fig. 4. X-ray diffractograms of the samples A0.86 (a), B2.8 (b) and C4.2 (c) after annealing at temperatures from 250 to 1500 °C (bottom to top). After heating to 450 °C, all three samples had transformed to the tetragonal phase. The transition to the monoclinic phase occurred after heating to 650 °C (A0.86) or 850 °C (B2.8 and C4.2).

densified and nonporous after calcination to 500 °C [35] or 700 °C [12,13].

It is noteworthy that after being heated to 850 °C, the mean particle diameters showed a slight increase. For B2.8 and C4.2, this increase in diameter is in accordance with the transformation of the particles from tetragonal to monoclinic as observed by XRD (Fig. 4). In bulk zirconia, this phase transformation is accompanied by a volume expansion of 3–5%. Moreover, it is noticeable that B2.8 and C4.2 show a much greater loss in diameter and mass than A0.86 (~35% against 13% by diameter and ~38% against 25% by mass). This might be due to the lower concentration of stabilizer used in the synthesis of A0.86 as opposed to the synthesis of B2.8 and C4.2, with stabilizer-to-zirconium molar ratios of 1:38 and 1:7.7, respectively.

For assembly into ordered, densely packed layers, it is important to consider the particle volumes which were calculated from the diameters and are shown in Fig. 3(b). The volume decreases after 450 °C were 35%, 75% and 72% for A0.86, B2.8 and C4.2, respectively, and remained relatively constant after further heating. In a layer of assembled particles such a significant loss in volume leads to cracking and the deterioration of the material's optical properties. Thus, it follows that pre-calcination to at least 450 °C prior to particle assembly is needed to avoid degradation of assembled layers at high temperatures.

3.2.2. Particle morphology and stability

For high-temperature applications, it is crucial to understand the effects of grain growth and phase transformations on the shape and stability of the particles. Additionally, as the submicron and microparticles are composed of smaller primary zirconia particles, it is vital to understand the effects of this morphology on the processability and stability of the particles as a function of temperature. Thus, A0.86, B2.8 and C4.2 were calcined at 250, 450, 650 and 850 °C for 1 h each and at 1200 and 1500 °C for 3 h each. The crystal structures, morphologies, and the stability of the particles to resuspension were investigated *ex situ* after cooling to room temperature.

The resulting phases were determined *via* X-ray diffraction. The diffractograms of the particles are shown in Fig. 4 as a function of calcination temperature. The as-synthesized particles were amorphous. Two phase transformations were observed with increasing calcination temperature. The first one was a transformation from the amorphous state to crystalline tetragonal zirconia, which occurred between 250 and 450 °C for all particle sizes. This is in agreement with the literature [36,40]. The second phase transformation was from tetragonal to monoclinic zirconia, which occurred after calcination at 650 °C for A0.86 and at 850 °C for both B2.8 and C4.2. This transition from the amorphous to the metastable high-temperature tetragonal phase and then to the thermodynamically stable monoclinic phase only after heating at higher temperatures is common and has been reported for zirconia microparticles [3,25,33,35,36,40,45–47] and nanoparticles [40,48–53].

Concerning the first phase transformation, it is commonly accepted that the local coordination environment and short-range order in the amorphous phase is more similar to the tetragonal rather than the monoclinic polymorph [40,48,50,54,55]. Thus, initial crystallization yields the metastable tetragonal phase. Keramidas et al. [49] further argued that the material is not truly amorphous to begin with. They observed that Raman spectra exhibited bands characteristic of the tetragonal phase, and electron diffraction indicated that the material is instead composed of 1.5–3.0 nm grains (30–200 unit cells) of a tetragonal-like phase.

Concerning the second phase transformation, the microspheres, B2.8 and C4.2, exhibited a higher transformation temperature when compared to the submicron spheres, A0.86. Sample A0.86 had transformed to the monoclinic phase after calcination at 650 °C, while both samples B2.8 and C4.2 remained tetragonal at this temperature. Samples B2.8 and C4.2 became monoclinic only after calcination at 850 °C, with a residual fraction of tetragonal phase remaining in both samples. These transformation temperatures are consistent with the literature, where a range between 600 and 800 °C is reported [36,40]. One possible explanation for the shift in transformation temperature between the particles is that they are composed of different crystallite sizes as a result of their different syntheses. Below a critical grain size, tetragonal rather than monoclinic becomes the thermodynamically preferred phase due to differences in the surface energies of the polymorphs. This critical size has been reported to be typically of the order of 10–20 nm but can vary up to 45 nm [40,48,52,56]. The crystallites that the particles are composed of can be seen in high-resolution SEM images (see Supplementary Material – Fig. S4) and their sizes were calculated from the XRDs using the Scherrer equation (Supplementary Material, Table S1). In general, it was found that the initial tetragonal crystallite size in the submicron particles at 450 °C (35 nm for A0.86) was much larger than in the microparticles (11 to 14 nm for B2.8 and C4.2). These values are above the typical critical grain size in the case of the A0.86 particles but are at or below in the case of the B2.8 and C4.2 particles, possibly explaining their differences in phase stability. The eventual transformation of B2.8 and C4.2 to the monoclinic phase at 850 °C was accompanied with grain growth to 31 and 27 nm, respectively. A more detailed analysis of the crystallite size measured *in situ* during heating and cooling is presented below. Alternatively, the shift in transformation temperature may be accounted for solely by the more aggregated nature of the larger microparticles. The microparticles consist of a larger number of grains than the submicron

particles, which results in a larger fraction of grains being confined inside the particle. Shukla and Seal have observed that the critical size increases when isolated nanoparticles become part of an aggregated particle due to interfacial and strain energy contributions [40]. Thus, the larger B2.8 and C4.2 particles could have a higher critical crystallite size, and the transformation would shift to higher temperatures where sufficient grain growth can occur. Together, the net shift in transformation temperature in the larger microparticles is most likely due to both their smaller primary crystallite size coupled with an increase in critical grain size.

The morphologies of the particles after calcination were investigated using SEM and are shown in Fig. 5. The stability of the particles to resuspension in ethanol *via* ultrasonication was also investigated. Independent of size, all of the as-synthesized particles sediment within one day in ethanol due to their high density but can be readily resuspended simply by shaking. After calcination at 450 °C and transformation into the tetragonal phase, particles of all sizes still display smooth surfaces and can be resuspended in ethanol *via* ultrasonication over the course of a few minutes without any particle destruction. After calcination to 850 °C, all particles were composed of small crystallites or grains as shown in the insets of Fig. 5. For A0.86, this led to destabilization and disintegration of particles after ultrasonication in ethanol. Conversely, both B2.8 and C4.2 were readily resuspended this way without disintegration. After calcination at 1200 °C, large crystalline features with sizes ranging from 300 to 1200 or 1600 nm were observed for A0.86 and B2.8, respectively (Fig. 5). The occurrence of these large crystallites causes the particles to completely lose their spherical shape and structural integrity. C4.2 formed spheres consisting of large grains with sizes from 200 to 750 nm, most of which were not stable to resuspension via ultrasonication. Lastly, after heating to 1500 °C, all samples had transformed into large grains with sizes ranging from 1 to 7 μm (Fig. 5). No intact particles were found. The grains also became more faceted. Texturing was observed *via* XRD (Fig. 4). While still monoclinic, the peak intensities deviated from the usual monoclinic peak ratios, with an increase in first the (111) orientation and then the (002) orientation at the expense of the $(11\bar{1})$ orientation.

In all experiments described above the calcination temperatures were set using heating ramps of 5 °C/min (see Supplementary Material). To test the influence of a reduced heating rate on the stability and morphology of the particles, some experiments were repeated with a heating rate of 2 °C/min. The findings of these experiments were essentially the same as described above. However, the tendency of particle disintegration after heating to 850 °C (and resuspension) was somewhat reduced in the case of the submicron particles. Similarly, the spherical shape of the 2.8 μm particles was better preserved after heating to 1200 °C, though significant grain coarsening was observed, as in the case of the faster heating rate. After heating the submicron particles to 1200 °C and the microparticles to 1500 °C, they disintegrated and lost their spherical appearance, as observed in the case of the faster heating rate. SEM images of samples heated at the slower rate are provided in the Supplementary Material, Fig. S8.

3.3. In situ experiments

As the *ex situ* experiments only provided information about the phases and morphologies present after cooling to room temperature, *in situ* high-energy X-ray diffraction experiments were performed to study the phase behavior, crystallite growth and microstrain of the particles as a function of the actual temperature. The three particle samples D0.81, E2.8 and F4.3 were heated up to a temperature of 1170 °C. In order to investigate any heating rate dependence of the phase transformations, each of the samples were heated with a slow ramp rate of 15 °C/min, and additionally, samples E2.8 and F4.3 were investigated with a fast ramp rate of 80–90 °C/min. The heating profiles and heating rates are shown in the Supplementary Material (Fig. S9 and Table S2). Selected diffractograms collected during the heating and cooling stages are provided in the Supplementary Material (Figs. S10–S15). The monoclinic weight percent fraction, the crystallite sizes for both the tetragonal and monoclinic phases and r.m.s. (root mean square) microstrain present in each phase were found by quantitative phase analysis using Rietveld refinement. Fig. 6(a)–(e) shows

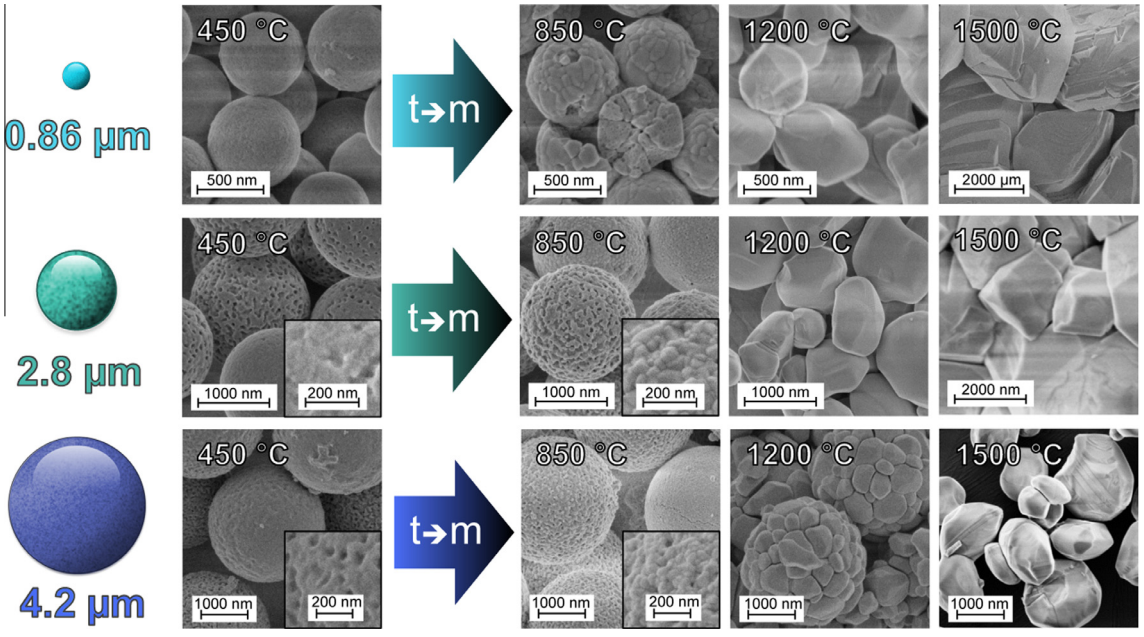

Fig. 5. SEM images of sample A0.86 (top row), B2.8 (center row) and C4.2 (bottom row) calcined at 450, 850, 1200 and 1500 °C (from left to right), grain sub-structure as inset (for B2.8 and C4.2). The martensitic tetragonal-to-monoclinic transformation occurred between heating to 450 and 850 °C. This was accompanied by a change in particle morphology, which was composed of small crystallites. Further heating to 1200 °C and 1500 °C led to increased grain growth which destabilized the particles.

these results for the three sizes of particles measured with the slow heating–cooling rate.

The first transformation of interest is the crystallization of the sample. Fig. 6(b) shows the size of the tetragonal crystallites as a function of temperature and particle size. It can be seen that crystallization from the amorphous phase to the tetragonal phase occurred at about 295 °C for E2.8 and 275 °C for F4.3, while D0.81 crystallized much later, at about 455 °C. This is in accord with the onset of the main weight loss event observed thermogravimetrically (Fig. 3(c)). After crystallization, all samples were tetragonal. Crystallization into the tetragonal phase between 270 and 455 °C is consistent with the findings of the *ex situ* experiments and the literature [36,40]. The initial tetragonal crystallite size of submicron sample D0.81 (28 nm) is larger than that of other two microparticle samples (8 and 6 nm for E2.8 and F4.3). This behavior is also consistent with the *ex situ* experiments. It was generally found that the lower crystallization temperature favored the nucleation of a larger number of crystallites for E2.8 and F4.3 and thus gave smaller crystallite sizes. Conversely, delaying crystallization to higher temperatures favored growth and thus provided fewer but larger crystallites, as was seen in sample D0.81. Moreover, crystallite growth was accompanied with a relief of microstrain in the material as is evident for the larger microparticles (Fig. 6(d)). The microstrain in the tetragonal grains was very high right after crystallization, which can be attributed to the short-range order of the initial amorphous state. This microstrain was relieved as the material transitioned into a long-range order state.

The second behavior of interest is the tetragonal-to-monoclinic transition. Three distinct regions are observable, as shown by the monoclinic weight fraction in Fig. 6(a). During heating, two increases in the fraction of the monoclinic phase with increasing temperature occurred and were separated by a plateau: the first from 450 to 650 °C and the second after 1000 °C. Between these regimes (650–1000 °C), the transformation is halted and a plateau of 20 and 30 wt% monoclinic is reached for D0.81 and F4.3 respectively. At the maximum temperature of 1170 °C, all samples displayed a mixed structure of monoclinic and tetragonal phases, but with strongly varying fractions for the different particle sizes. D0.81 and F4.3 reached 25 and 40 wt% monoclinic fractions, respectively. For E2.8, a less pronounced plateau was observed and the monoclinic phase increased continuously until it reached over 80 wt% at 1170 °C. The third phase transformation regime occurred upon cooling. The monoclinic fractions of D0.81 and F4.3 remained constant as the samples cooled until 800 and 600 °C, respectively, where they displayed a rapid increase in the monoclinic fraction, reaching 90 wt% at room temperature. Again, E2.8 seemed to deviate by displaying a small decrease in the monoclinic fraction, until it jumped discontinuously up to 90 wt% as well at about 600 °C.

While the tetragonal-to-monoclinic phase transformation upon cooling is well known, the transformation with heating is a matter of contention. In previous *in situ* XRD experiments conducted on zirconia nanoparticles precipitated from zirconium tetrachloride with ammonium hydroxide, a transition from the tetragonal to the monoclinic phase was not observed while the sample was being heated up, but only after cooling to 250 °C [50]. Other studies have found a partial transition to the monoclinic phase during heating, similar to this work [57,58]. Inspection of *in situ* results in this work reveals that upon heating the increase in monoclinic fraction tracks well with the increase of the tetragonal crystallite size. When the crystallite size stagnated, no increase of the monoclinic fraction was observed, but when the crystallite size increased, the monoclinic fraction grew as well. In order to assess the degree of statistical dependence between the monoclinic fraction and tetragonal grain size, the Pearson product-moment coefficient was determined for the two curves. The coefficient is

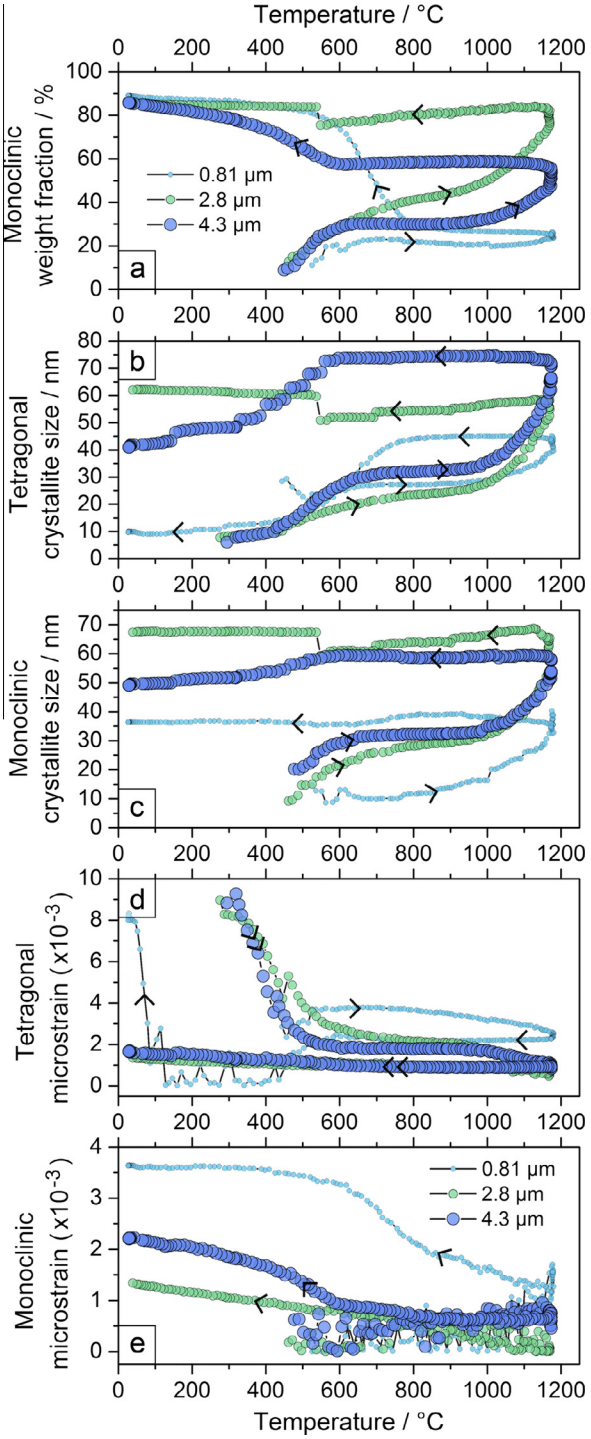

Fig. 6. Monoclinic weight fraction (a), crystallite size of tetragonal (b) and monoclinic (c) phases, and microstrain of tetragonal (d) and monoclinic (e) phases as a function of temperature for particle samples D0.81, E2.8 and F4.3 with a slow heating–cooling rate of 15 °C/min. Arrows indicate direction of heating and cooling.

a value between +1 and −1, where 1 is total positive correlation, 0 is no correlation, and −1 is total negative correlation. A Pearson coefficient of 0.96 and 0.97 was determined for E2.8 and F4.3 respectively, indicating a strong, positive correlation between the monoclinic fraction and the tetragonal grain size.

As stated above, two increases in the fraction of the monoclinic phase with increasing temperature occurred with heating. As the plateau in grain growth agrees well with the plateau in the phase transformation, it is likely that a change in growth mechanism

occurs with temperature. The results suggest that growth occurs at low temperature by a low activation energy mechanism (surface diffusion for example) until growth is exhausted, corresponding to the plateau. It was observed that the growth at low temperature from 450 to 650 °C follows the residual tetragonal microstrain present in the microparticles after crystallization from the amorphous to the tetragonal phase (Fig. 6(b) and (d)). Growth occurs as this microstrain is relieved. A Pearson coefficient of −0.89 and −0.97 was determined for E2.8 and F4.3, indicating a strong, negative correlation between the tetragonal grain size and tetragonal microstrain. When this strain plateaus, the first growth stage stagnates. Further growth can only then take place by a higher activation energy mechanism, which cannot start until higher temperatures are achieved (the second increase).

In order to gain more insight into this mechanism, a second set of experiments was conducted with a faster heating–cooling rate ranging between 80 and 90 °C/min. The results from quantitative phase analysis for samples E2.8 and F4.3 are shown in Fig. 7 and Fig. S16. The monoclinic weight percentage in the two samples showed consistently low values during the heating and through most of the cooling of the particles (⩽10 wt%). Only during cooling below 600 °C did both samples exhibit a significant phase transformation, reaching maximum values of about 70 wt% of the monoclinic phase at room temperature. In both the slow and the fast heating experiments, an increase in the monoclinic weight fraction at temperatures above 1000 °C coincided with an increase of the tetragonal grain size, but for the fast *in situ* experiment, the first stage of the monoclinic transformation at lower temperatures was not observed, even with a measured increase in grain size. When viewed together, it appears that there are in fact two domains and two different mechanisms during heating. We conclude that the heating rate appears to only influence the low temperature mechanism, which affects the initial formation of the monoclinic phase between the crystallization temperature and 600 °C, and after which the fraction is locked in until higher temperatures, where further grain growth occurs and the critical grain size mechanism takes over. The rate constant for the first mechanism must be slow. To give a sense of scale, the entire heating step to 1170 °C for the quick rate experiment was performed in ~15 min. This is the same time required to heat 200 degrees in the slow rate experiment from the crystallization temperature at 400 °C to the plateau at 600 °C. The quick heating resulted in the regime controlled by the first mechanism being bypassed into the regime dominated by the second mechanism before it could have an effect, and thus the monoclinic phase was only observed at higher temperatures. This is supported by the fact that it was observed that the tetragonal crystallite size after cooling was approximately 30–40 nm for E2.8 and F4.3 in the fast heating experiment, which is the same size the samples reached during the plateau between 600 and 1000 °C for both slow and fast heating. This is most likely the critical grain size for these two samples, as any grain growth exceeding this value coincided with a further transformation from the tetragonal to the monoclinic phase. It is noteworthy that E2.8 showed a deviating behavior in comparison to sample F4.3 in the slow heating experiments, but agrees well with sample F4.3 in the fast heating experiments. The differences in the behavior of the two samples may be due to factors which might not be as important in the fast heating, or more likely due to a measurement artifact such as movement of the powder in the beam, which cannot be completely excluded as the source of the discontinuity.

Additionally, the size of the tetragonal grains upon cooling to room temperature can be used to determine the critical crystallite size for phase transformation for the different particle sizes. Upon cooling, any tetragonal grains larger than this size should transform to monoclinic. Thus, the critical size was determined to

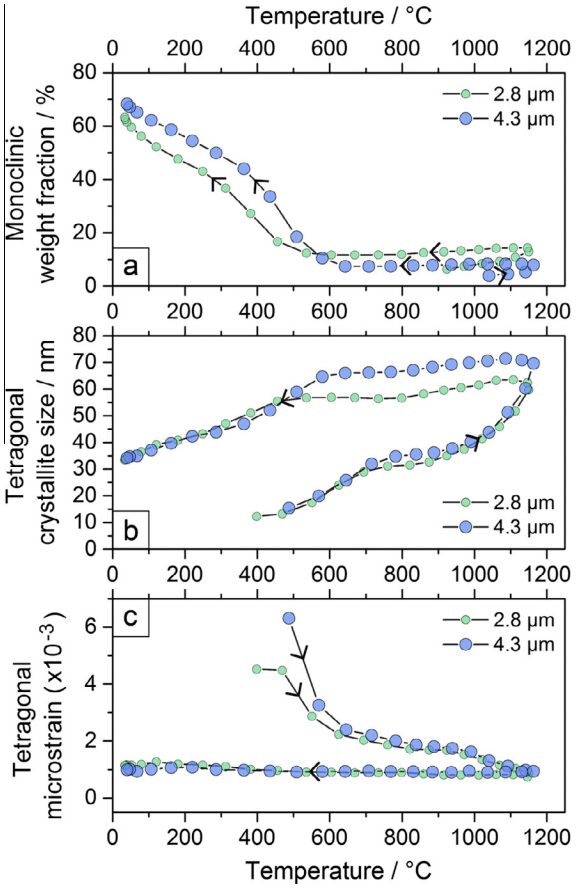

Fig. 7. Monoclinic weight fraction (a), crystallite size of tetragonal phases (b) and tetragonal microstrain (c) as a function of temperature for particle sizes E2.8 and F4.3 with a quick heating–cooling rate of 80–90 °C/min. Arrows indicate direction of heating and cooling.

be 10, 62 and 41 nm for particles D0.81, E2.8 and F4.3 respectively with the slow heating–cooling rate (Fig. 6(b)) and to be 35 nm for both particles E2.8 and F4.3 with the fast rate (Fig. 7(b)). The value for the sub-micron particles is consistent with the typically reported critical value for zirconia nanoparticles, while the values for the microparticles are consistent with those reported for aggregated nanoparticle systems. As noted in the *ex situ* discussion, Shukla and Seal have observed that the critical size increases when isolated nanoparticles become elements of an aggregated particle [40]. This conclusion is supported by this work. As a note, it is important to be careful when interpreting any correlation with tetragonal crystallite size when cooling the sample below 600 °C. A first glance would indicate that the tetragonal grains are shrinking with temperature. However, this is a counting artifact. As the larger tetragonal crystallites transform to monoclinic, they leave behind only the smaller tetragonal crystallites, which decreases the overall average tetragonal crystallite size as measured.

No such artifact exists for the monoclinic crystallite size (Fig. 6(c)). The monoclinic crystallite sizes remained relatively constant for each particle as they formed upon cooling. It is important to note that the steady-state sizes of the tetragonal grains during cooling, as given by the plateau region in the cooling curve before the monoclinic transformation begins (until 800 °C for D0.81 and 600 °C for E2.8 and F4.3), were similar (differing between 5 and 20 nm) to the resulting monoclinic sizes for each sample. For example, in the case of D0.81, the steady-state tetragonal size of ~40 nm until cooling to 800 °C yielded monoclinic grains of ~35 nm. Thus, the size of the tetragonal grains before

transformation during cooling is a good indicator of the final monoclinic grain size.

The monoclinic microstrain (Fig. 6(e)) behaved the opposite of the tetragonal microstrain. During heating, the monoclinic microstrain was low and displayed a high uncertainty. During cooling, the microstrain slowly increased. It was noticeable that the final monoclinic microstrain was the highest for sample D0.81 and that it increased most between cooling from 800 and 600 °C, which corresponded to the temperature region where this sample displayed its most pronounced transformation from the tetragonal to the monoclinic phase. D0.81 also displayed a considerable increase in tetragonal microstrain when cooling below 100 °C. Additionally, it was the only sample that was already unstable and broke apart after transforming to the monoclinic phase. The breaking of the particles, which inhibits their resuspension for processing and leads to a loss of properties in operation, is thus most likely related to a high build-up of microstrain in the particles caused by the martensitic volume expansion. Conversely, only a modest increase of the monoclinic microstrain and a slight increase in tetragonal microstrain during cooling were observed for E2.8 and F4.3. The larger microparticles exhibited a lower final microstrain overall and thus greater stability.

3.4. Yttria-stabilized particles

Given the thermal instabilities observed for the pure zirconia particles at temperatures higher than 1200 °C, a synthetic route was developed for zirconia microspheres stabilized *via* yttria-doping and the stability of these particles at high-temperatures was evaluated. Yttria-stabilized zirconia microspheres were prepared in a method similar to the large microparticle synthesis using yttrium isopropoxide as an yttrium precursor. It was added directly to the zirconium n-propoxide solution in order to achieve a target composition of 8 at.% of Y/(Zr + Y), which is known to stabilize the tetragonal phase for bulk YSZ at room temperature [39]. Synthesis and work-up yielded particles with a 2.3 μm diameter and a 6% standard deviation (Fig. 8(a)). In comparison to the undoped zirconia particles the yttria-stabilized sample contains more aggregated particles, predominantly in the form of dimers. These aggregates are most likely formed during the ageing time due to a higher surface reactivity of these particles. Uchiyama et al. [39] and Keshmiri et al. [38] both synthesized submicron yttria-doped particles and heated them to temperatures of up to 1000 °C, after which the particles had crystallized in the tetragonal phase. To the best of our knowledge, the particles presented in this study are the largest monodisperse YSZ microparticles synthesized to date. For the first time, the crystal structure, the morphology and the stability of yttria-stabilized particles was investigated after heating to temperatures up to 1500 °C. Furthermore, the effect of prolonged heat exposure was examined by calcining the particles at 1200 °C for 20 h.

After calcination at 1200 °C the particles shrank to a final particle size of 1.5 μm. The composition of the calcined microspheres was determined by optical emission spectroscopy (ICP-OES) and found to be 8.4 ± 0.1 at.% Y/(Zr + Y), which is consistent with the occurrence of the tetragonal phase. This value agrees well with the reagent ratio, indicating successful incorporation of the dopant during synthesis. XRD confirmed that the tetragonal phase remained stable after 3 h calcination at 1200 °C and cooling (Fig. 8(c)) using the same heating profile that the undoped particles were subjected to. The SEM image in Fig. 8(b) shows the morphology of the particles after heating to 1200 °C. The particles are composed of smaller grains, but, in contrast to C4.2, which had a similar morphology after the heat treatment, this did not cause the yttria-doped particles to destabilize. They were stable to resuspension via ultrasonication. For comparison, the undoped zirconia

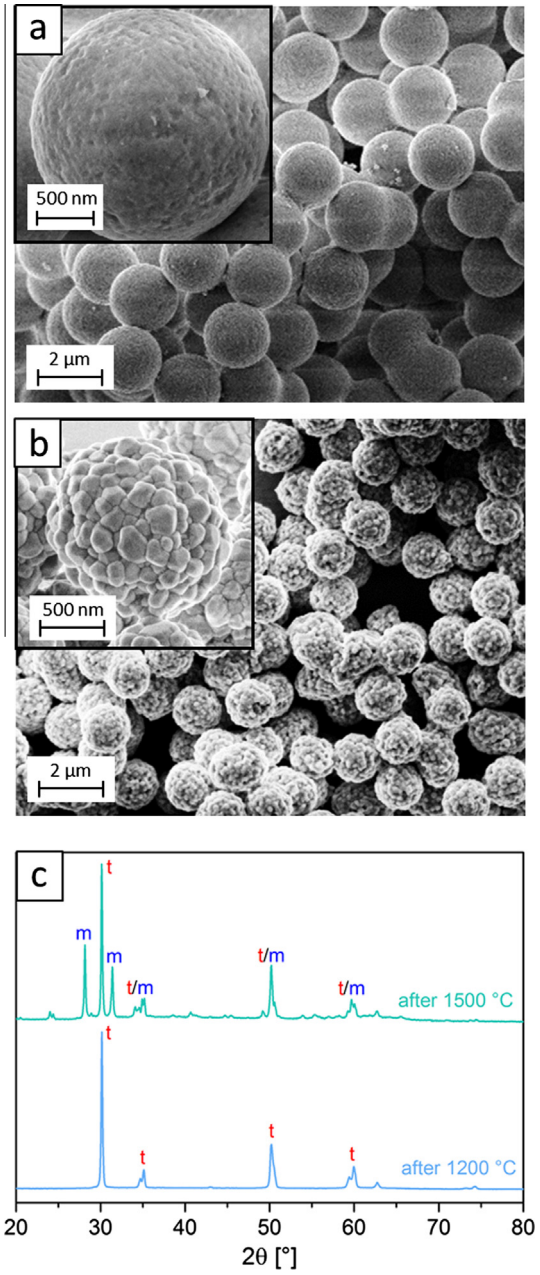

Fig. 8. Yttria-stabilized zirconia particles as synthesized (a) and after heating to 1200 °C (b) with the heating profile shown in the Supplementary Material (Fig. S6), and X-ray diffractograms for the yttria-stabilized particles after heating to 1200 and 1500 °C (c). After heating to 1200 °C, the particles had a grainy morphology but were stable to resuspension via ultrasonication.

microspheres of similar size (A0.86 and B2.8) had become monoclinic and had broken apart under the same conditions, as is shown in Fig. 5. Even after heating to 1500 °C, the samples mostly remained tetragonal with a small fraction of the monoclinic phase (Fig. 8(c)). However, the increased grain growth caused the destabilization of the particles (see Supplementary Material – Fig. S17). The crystallite sizes in the particles were calculated from the XRD with the Scherrer equation and it was shown that the values obtained were consistently smaller for the yttria-doped particles than for the three undoped zirconia particle samples A0.86, B2.8 and C4.2 (see Supplementary Material – Table S1). After heating to 850 °C, the yttria-doped particles had a crystallite size of 16 nm, while the undoped particles exhibited crystallite sizes ranging from 27 to 41 nm. After heating to 1200 °C, the crystallites had

grown to approximately 80 nm in the yttria-doped particles and exceeded 80 for the undoped samples.

Finally, both the yttria-stabilized particles and undoped sample E2.8 were calcined at 1200 °C for 20 h. Their crystal structures were analysed *via* XRD and their resuspendability was tested by ultrasonic dispersion. The yttria-stabilized particles had a similar morphology as the sample heated at 1200 °C for only 3 h and were stable to resuspension, although some particle breaking was observed. XRD analysis showed that they were still mostly tetragonal but with a small monoclinic fraction appearing. Conversely, the undoped sample consisted of much larger grains and, as expected, had fully transformed into the monoclinic phase. SEM micrographs and X-ray diffractograms are provided in the Supplementary Material (Fig. S18).

4. Conclusion

Spherical zirconia submicron and microparticles were reproducibly synthesized with high monodispersities by a sol–gel process using fatty acids as stabilizers. Upon heating, the particles transformed from the amorphous to the tetragonal phase at 250–450 °C and to the monoclinic phase after calcination above 450 or 650 °C, depending on the synthesis route. After heating to 450 °C the particles displayed considerable shrinkage with a volume loss of up to 75%. The change in particle size when heating above 450 °C was negligible. With increasing calcination temperature, grain growth occurred in the particles and caused the submicron particles to become destabilized and to break apart. Larger microparticles were stable in size and shape up to a calcination temperature of at least 850 °C, but destabilized when heated to 1200 °C. *In situ* high-energy X-ray diffraction experiments showed that larger microparticles, synthesized using zirconium n-propoxide and a higher stabilizer concentration, consisted of smaller grains which crystallized at lower temperatures. The submicron particles made with zirconium n-tetrabutoxide and a lower stabilizer concentration were composed of comparatively larger grains which crystallized at higher temperatures. We conclude that earlier crystallization and smaller initial grain size coincide with a higher temperature stability of the zirconia particles. It is unclear what causes the earlier crystallization but it is most likely related to the synthetic mechanism and the choice of precursor material. Doping the microparticles with yttria proved to be a convenient way of stabilizing the tetragonal phase and suppressing grain growth, improving the high-temperature stability of the particles. The monodisperse, spherical particles synthesized in this work are processable for a number of applications, such as in chromatography and in high-temperature photonic materials. Currently we are working on the development of high-temperature stable zirconia particles doped with various metal ions in order to inhibit grain growth and prevent the partial transformation to the monoclinic phase after heating to temperatures up to ~1200 °C.

Acknowledgments

The authors gratefully acknowledge financial support from the German Research Foundation (DFG) via SFB 986 "Tailor-Made Multi-Scale Materials Systems: M^3", projects C5, C6 and Z2. Parts of this research were carried out at the light source PETRA III at DESY, a member of the Helmholtz Association (HGF). We would like to thank Lars Lottermoser, Daniel Ostach, René Kirchhof, Norbert Schell, and Ursula Tietze for setting up the experiment at beamline P07 (HEMS) of Helmholtz-Zentrum Geesthacht. We thank Malte Blankenburg for assistance with the quantitative phase analysis. Furthermore, we thank Frank Meyberg and the analytics department for conducting the ICP-OES measurements, Robert Schön for measuring HR-SEM images and Almut Barck for the *ex situ* XRD measurements. We thank Adam Steiger for assisting with proof reading the manuscript.

Appendix A. Supplementary material

Supplementary data associated with this article can be found, in the online version, at http://dx.doi.org/10.1016/j.jcis.2015.02.049.

References

[1] I. Freris, P. Riello, F. Enrichi, D. Cristofori, A. Benedetti, Opt. Mater. 33 (2011) 1745–1752, http://dx.doi.org/10.1016/j.optmat.2011.06.010.
[2] J. He, J. Chen, L. Ren, Y. Wang, C. Teng, M. Hong, et al., ACS Appl. Mater. Interfaces 6 (2014) 2718–2725, http://dx.doi.org/10.1021/am405202d.
[3] H. Uchiyama, K. Takagi, H. Kozuka, Colloids Surf. A Physicochem. Eng. Asp. 403 (2012) 121–128, http://dx.doi.org/10.1016/j.colsurfa.2012.03.065.
[4] T. Koch, P. Ziemann, Appl. Surf. Sci. 99 (1996) 51–57, http://dx.doi.org/10.1016/0169-4332(95)00512-9.
[5] J.H. Shim, C. Chao, H. Huang, F.B. Prinz, Chem. Mater. 19 (2007) 3850–3854, http://dx.doi.org/10.1021/cm070913t.
[6] T. Miller, V. Grassian, J. Am. Chem. Soc. 117 (1995) 10969–10975, http://dx.doi.org/10.1021/ja00149a020.
[7] Y. Li, D. He, Z. Cheng, C. Su, J. Li, Q. Zhu, J. Mol. Catal. A Chem. 175 (2001) 267–275, http://dx.doi.org/10.1016/S1381-1169(01)00233-3.
[8] D. Chen, L. Cao, F. Huang, P. Imperia, Y.-B. Cheng, R.A. Caruso, J. Am. Chem. Soc. 132 (2010) 4438–4444, http://dx.doi.org/10.1021/ja100040p.
[9] D. Lu, J. Wang, L. Wang, D. Du, C. Timchalk, R. Barry, et al., Adv. Funct. Mater. 21 (2011) 4371–4378, http://dx.doi.org/10.1002/adfm.201100616.
[10] M. Zhou, A. Ahmad, Mater. Res. Bull. 41 (2006) 690–696, http://dx.doi.org/10.1016/j.materresbull.2005.10.018.
[11] A. Subramanian, P.W. Carr, C.V. McNeff, J. Chromatogr. A 890 (2000) 15–23, http://dx.doi.org/10.1016/S0021-9673(00)00289-2.
[12] B. Yan, C. McNeff, F. Chen, J. Am. Ceram. Soc. 27 (2001) 1721–1727, http://dx.doi.org/10.1111/j.1151-2916.2001.tb00905.x.
[13] B. Yan, C.V. McNeff, P.W. Carr, A.V. McCormick, J. Am. Ceram. Soc. 88 (2005) 707–713, http://dx.doi.org/10.1111/j.1551-2916.2005.00133.x.
[14] A. Pattanayak, A. Subramanian, Powder Technol. 192 (2009) 359–366, http://dx.doi.org/10.1016/j.powtec.2009.01.023.
[15] A. Pattanayak, A. Subramanian, Int. J. Appl. Ceram. Technol. 8 (2011) 94–111, http://dx.doi.org/10.1111/j.1744-7402.2009.02410.x.
[16] G. von Freymann, V. Kitaev, B.V. Lotsch, G.A. Ozin, Chem. Soc. Rev. 42 (2013) 2528–2554, http://dx.doi.org/10.1039/c2cs35309a.
[17] P.D. García, R. Sapienza, Á. Blanco, C. López, Adv. Mater. 19 (2007) 2597–2602, http://dx.doi.org/10.1002/adma.200602426.
[18] P.D. García, R. Sapienza, C. López, Adv. Mater. 22 (2010) 12–19, http://dx.doi.org/10.1002/adma.200900827.
[19] D.R. Clarke, C.G. Levi, Annu. Rev. Mater. Res. 33 (2003) 383–417, http://dx.doi.org/10.1146/annurev.matsci.33.011403.113718.
[20] Y. Takeoka, J. Mater. Chem. C 1 (2013) 5993–6164, http://dx.doi.org/10.1039/c3tc30885e.
[21] P.N. Dyachenko, A.Y. Petrov, M. Eich, Appl. Phys. Lett. 103 (2013) 211105, http://dx.doi.org/10.1063/1.4832071.
[22] P.N. Dyachenko, J.J. do Rosário, E.W. Leib, A.Y. Petrov, R. Kubrin, G.A. Schneider, et al., ACS Photonics 1 (2014) 1127–1133, http://dx.doi.org/10.1021/ph500224r.
[23] R.H.J. Hannink, P.M. Kelly, B.C. Muddle, J. Am. Ceram. Soc. 83 (2000) 461–487, http://dx.doi.org/10.1111/j.1151-2916.2000.tb01221.x.
[24] M. Dechamps, B. Djuricic, S. Pickering, J. Am. Ceram. Soc. 78 (1995) 2873–2880, http://dx.doi.org/10.1111/j.1151-2916.1995.tb09058.x.
[25] Y.T. Moon, H.K. Park, D.K. Kim, C.H. Kim, I.-S. Seog, J. Am. Ceram. Soc. 78 (1995) 2690–2694, http://dx.doi.org/10.1111/j.1151-2916.1995.tb08042.x.
[26] Y.T. Moon, D.K. Kim, C.H. Kim, J. Am. Ceram. Soc. 78 (1995) 1103–1106, http://dx.doi.org/10.1111/j.1151-2916.1995.tb08448.x.
[27] K. Lee, A. Sathyagal, P.W. Carr, A.V. McCormick, J. Am. Ceram. Soc. 42 (1999) 338–342, http://dx.doi.org/10.1111/j.1551-2916.1999.tb20067.x.
[28] M.J. Annen, R. Kizhappali, P.W. Carr, A. McCormick, J. Mater. Sci. 29 (1994) 6123–6130, http://dx.doi.org/10.1007/BF00354551.
[29] L. Sun, M.J. Annen, F. Lorenzano-Porras, P.W. Carr, A.V. McCormick, J. Colloid Interface Sci. 163 (1994) 464–473, http://dx.doi.org/10.1006/jcis.1994.1125.
[30] A.N. Sathyagal, P.W. Carr, A.V. McCormick, J. Colloid Interface Sci. 219 (1999) 20–30, http://dx.doi.org/10.1006/jcis.1999.6447.
[31] B. Fegley, E. Barringer, Better Ceram. Through Chem. Mat. Res. Soc. Symp. Proc. 32 (1984) 187–197. http://journals.cambridge.org/production/action/cjoGetFulltext?fulltextid=8099091.
[32] B. Fegley, P. White, H. Bowen, Am. Ceram. Soc. Bull. 64 (1985) 1115–1120.
[33] T. Ogihara, N. Mizutani, M. Kato, Ceram. Int. 13 (1987) 35–40. http://www.sciencedirect.com/science/article/pii/0272884287900368.
[34] T. Ogihara, N. Mizutani, M. Kato, J. Am. Ceram. Soc. 26 (1989) 421–426, http://dx.doi.org/10.1111/j.1151-2916.1989.tb06146.x.
[35] L. Lerot, F. Legrand, P. De Bruycker, J. Mater. Sci. 26 (1991) 2353–2358, http://dx.doi.org/10.1007/BF01130181.

[36] J. Widoniak, S. Eiden-Assmann, G. Maret, Eur. J. Inorg. Chem. 15 (2005) 3149–3155, http://dx.doi.org/10.1002/ejic.200401025.
[37] J. Widoniak, S. Eiden-Assmann, G. Maret, Colloids Surfaces A Physicochem. Eng. Asp. 270 (2005) 329–334, http://dx.doi.org/10.1016/j.colsurfa.2005.09.014.
[38] M. Keshmiri, O. Kesler, Acta Mater. 54 (2006) 4149–4157, http://dx.doi.org/10.1016/j.actamat.2006.05.010.
[39] K. Uchiyama, T. Ogihara, T. Ikemoto, J. Mater. Sci. 22 (1987) 4343–4347, http://dx.doi.org/10.1007/BF01132027.
[40] S. Shukla, S. Seal, J. Phys. Chem. B. 108 (2004) 3395–3399, http://dx.doi.org/10.1021/jp037532x.
[41] M. Ferrari, L. Lutterotti, J. Appl. Phys. 76 (1994) 7246–7255, http://dx.doi.org/10.1063/1.358006.
[42] H. Kumazawa, Y. Hori, E. Sada, Chem. Eng. J. 51 (1993) 129–133. http://www.sciencedirect.com/science/article/pii/030094679380023H.
[43] G. Chuah, Catal. Today 49 (1999) 131–139, http://dx.doi.org/10.1016/S0920-5861(98)00417-9.
[44] M. Tahmasebpour, A.A. Babaluo, M.K.R. Aghjeh, J. Eur. Ceram. Soc. 28 (2008) 773–778, http://dx.doi.org/10.1016/j.jeurceramsoc.2007.09.018.
[45] O. Van Cantfort, B. Michaux, R. Pirard, J.P. Pirard, A.J. Lecloux, J. Sol–Gel Sci. Technol. 8 (1997) 207–211, http://dx.doi.org/10.1007/BF02436842.
[46] M.Y. Ghotbi, V. Nasiri, M. Rafiee, J. Colloid Interface Sci. 389 (2013) 121–125, http://dx.doi.org/10.1016/j.jcis.2012.09.013.
[47] M.A. Blesa, A.J.G. Maroto, S.I. Passaggio, N.E. Figliolia, G. Rigotti, J. Mater. Sci. 20 (1985) 4601–4609, http://dx.doi.org/10.1007/BF00559350.
[48] T. Chraska, A.H. King, C.C. Berndt, Mater. Sci. Eng. A 286 (2000) 169–178, http://dx.doi.org/10.1016/S0921-5093(00)00625-0.
[49] V. Keramidas, W. White, J. Am. Ceram. Soc. 57 (1974) 22–24, http://dx.doi.org/10.1111/j.1151-2916.1974.tb11355.x.
[50] R. Srinivasan, B.H. Davis, O.B. Cavin, C.R. Hubbard, J. Am. Ceram. Soc. 75 (1992) 1217–1222, http://dx.doi.org/10.1111/j.1151-2916.1992.tb05560.x.
[51] R. Srinivasan, R.J. De Angelis, G. Ice, B.H. Davis, J. Mater. Res. 6 (2011) 1287–1292, http://dx.doi.org/10.1557/JMR.1991.1287.
[52] R. Garvie, M. Goss, J. Mater. Sci. 21 (1986) 1253–1257, http://dx.doi.org/10.1007/BF00553259.
[53] E. Tani, M. Yoshimura, S. Somiya, J. Am. Ceram. Soc. 66 (1983) 13–16, http://dx.doi.org/10.1111/j.1151-2916.1983.tb09958.x.
[54] J. Livage, C. Mazieres, J. Am. Ceram. Soc. 51 (1968) 349–353, http://dx.doi.org/10.1111/j.1151-2916.1968.tb15952.x.
[55] F. Zhang, P.J. Chupas, S.L.A. Lui, J.C. Hanson, W.a. Caliebe, P.L. Lee, et al., Chem. Mater. 19 (2007) 3118–3126, http://dx.doi.org/10.1021/cm061739w.
[56] A. Navrotsky, J. Mater. Chem. 15 (2005) 1883–1890, http://dx.doi.org/10.1039/b417143h.
[57] M. Bhagwat, V. Ramaswamy, Mater. Res. Bull. 39 (2004) 1627–1640, http://dx.doi.org/10.1016/j.materresbull.2004.05.008.
[58] M. Dapiaggi, F. Maglia, I. Tredici, B. Maroni, G. Borghini, U.A. Tamburini, J. Phys. Chem. Solids 71 (2010) 1038–1041, http://dx.doi.org/10.1016/j.jpcs.2010.03.002.